THE JOURNAL OF PHYSICAL CHEMISTRY LETTERS
A JOURNAL OF THE AMERICAN CHEMICAL SOCIETY

pubs.acs.org/JPCL

Letter

Physical Insights on the Thermoelectric Performance of Cs_2SnBr_6 with Ultralow Lattice Thermal Conductivity

Xiangyu Zeng, Jutao Jiang, Guangming Niu, Laizhi Sui,* Yutong Zhang, Xiaowei Wang, Xin Liu, Anmin Chen,* Mingxing Jin, and Kaijun Yuan*

Cite This: *J. Phys. Chem. Lett.* 2022, 13, 9736−9744

Read Online

ACCESS | Metrics & More | Article Recommendations | Supporting Information

ABSTRACT: This study has investigated the microscopic mechanisms of ultralow lattice thermal conductivity by the first-principles density functional theory. By solving the phonon Boltzmann equation iteratively, we find that the thermal conductivity of the lattice is abnormally low and that glass like heat transfer behavior occurs. Therefore, in addition to the contribution about the particle-like propagation to heat transport, the off-diagonal elements of the heat-flux operator through wave-like interbranch tunneling of phonon modes are also considered. The results provided new insights into the minimum thermal conductivity (κ_L) for Cs_2SnBr_6 (0.17 W m^{-1} K^{-1} at 450 K). It was also found that polar optical phonon scattering severely affects carrier lifetime. In addition, an impressive thermoelectric figure of merit of 0.55 at 450 K for Cs_2SnBr_6 was obtained in the case of doping *p*-type carriers. The study helps us understand the ultralow κ_L in complex crystals with strong anharmonicity and find that Cs_2SnBr_6 is a new and promising thermoelectric material.

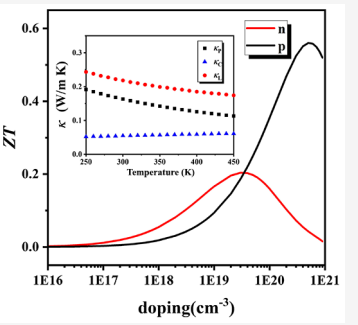

In the context of quantifying the performance of thermoelectric materials, establishing the connections between the transport properties and the thermoelectric figure of merit (ZT) is the most effective way to find new thermoelectric materials. The competence of thermoelectric materials is determined by a dimensionless figure of merit:[1]

$$ZT = \frac{S^2\sigma}{(\kappa_e + \kappa_L)}T \quad (1)$$

where S is the Seebeck coefficient and σ is the electrical conductivity and κ_e and κ_L are the electronic and lattice thermal conductivities, respectively. Thermoelectric materials interconvert heat and electrical energy for power generation or refrigeration. The material with good thermoelectric properties requires high current, high voltage, and poor thermal conductivity in electron−phonon transport. The strong mutually restricted relationship between σ, S, and κ_e makes it extremely difficult to increase the ZT value. Consequently, reducing lattice thermal conductivity (κ_L) is necessary to achieve high thermoelectric performance.

Recently, vacancy-ordered double perovskites A_2BX_6 have been gaining attention for thermoelectric energy conversion due to unique structural attributes and ultralow lattice thermal conductivity.[2−6] Researchers have found that Cs_2SnI_6 is a good *n*-type thermoelectric material due to its lattice thermal conductivity of 0.29−0.22 W m^{-1} K^{-1} in an air-stable environment.[3] Sajjad et al. studied the electron and phonon transport properties of Cs_2PtI_6 and found that heavy elements can act as phonons to effectively suppress the lattice thermal conductivity (0.15 W m^{-1} K^{-1} at room temperature).[5] However, a constant relaxation time was considered to estimate the figure of merit in their theory. Chen et al. found that power factors calculated with a constant and universal relaxation time approximation show much poorer agreement with the experiment.[7] This limits the electron transport by the simple model, obtaining results with large errors.[8] Xie et al. calculated relaxation time based on the deformation potential (DP) theory, leading to the ultrahigh figure of merits being close to 4.01 and 3.34 monolayer SnI_2 at 800 K.[9] In this work, we employ a more comprehensive carrier transport model to calculate the relaxation time, involving acoustic deformation potential (ADP), polar-optical phonon (POP), and ionized impurity (IMP) scattering processes. To date, there are few reports on the calculated thermoelectric properties of tin-based perovskite. Therefore, this study focuses on the thermoelectric properties of Cs_2SnBr_6.

This work combined density functional theory with the Boltzmann transport equation to investigate the thermoelectric properties of Cs_2SnBr_6. The material's phonon transport properties including Grüneisen parameter, phonon lifetime, three-phonon scattering phase space, mean free path (MFP), and lattice thermal conductivity were provided. The lattice thermal conductivity of Cs_2SnBr_6 was abnormally low (0.11W

Received: July 29, 2022
Accepted: October 3, 2022
Published: October 12, 2022

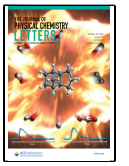

https://doi.org/10.1021/acs.jpclett.2c02350
J. Phys. Chem. Lett. 2022, 13, 9736−9744

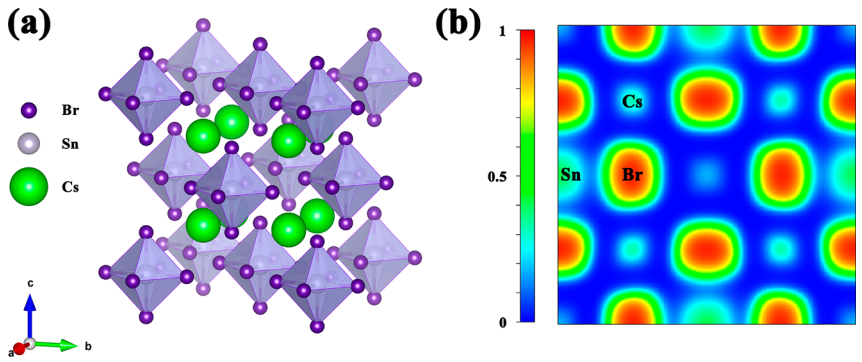

Figure 1. (a) Crystal structure of Cs_2SnBr_6; the $[SnBr_6]^{2-}$ octahedra are shaded, with the Br atom on the corners. The Cs cations are in the void between $[SnBr_6]^{2-}$ octahedra. Cs, Sn, and Br atoms are shown as green, gray, and purple spheres, respectively. (b) ELF projected on the planes (010). Color bar represents the value of the ELF corresponding to different bondings. Within the color maps, red indicates regions of strong electron localization, whereas blue indicates delocalized regions.

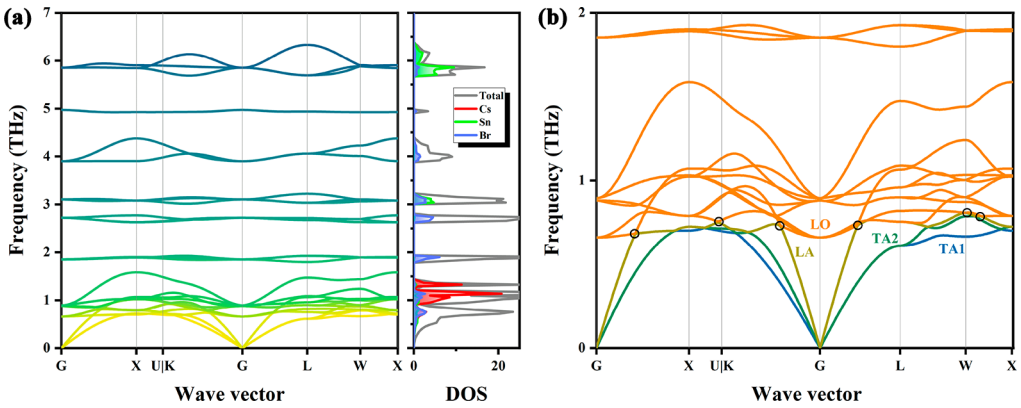

Figure 2. (a) Phonon dispersions and atom-projected phonon density of states (PDOS). (b) Zoomed view of phonon dispersion in the low-frequency region, where the first three low-frequency phonon modes are acoustic branches, which are shown in yellow-green, green, and blue, respectively, and the optical phonon branches are represented with orange curves.

m^{-1} K^{-1} ~ 450 K) by solving the phonon Boltzmann transport equation, and glass-like heat transfer behavior appeared. Therefore, in addition to considering the contribution of crystal periodicity to heat transfer, we also consider the lack of the periodic heat transfer mechanism (wave-like conduction in glass); that is, heat is transmitted through phonon mode vibration coupling. We use the Wigner transport equation to solve the thermal conductivity tensor accounting for the particle-like propagation and wave-like tunneling of phonons. Finally, the lattice thermal conductivity of Cs_2SnBr_6 is corrected as 0.17 W m^{-1} K^{-1} at 450 K. The ultralow lattice thermal conductivity originated from its strong anharmonicity, such as softened acoustic modes, weak bonding interactions, etc. An impressive ZT of 0.55 at the considered carrier concentration and temperature has been revealed, which suggests the high thermoelectric performance of Cs_2SnBr_6.

Crystalline solids with unique structural attributes and chemical bonding have great potential in the application of thermoelectric materials. Lead-free vacancy-ordered double perovskite Cs_2SnBr_6 is face-centered cubic (space group $Fm3m$) with only nine atoms in its primitive unit cell, as shown in Figure 1(a). It can be seen that Sn^{4+} is bonded to six equivalent Br^- atoms to form $[SnBr_6]^{2-}$ octahedra. For the complex crystal structure, we have analyzed the electron distribution in Cs_2SnBr_6 with the aid of the real-space descriptors electron localization function (ELF). Figure 1(b) shows that the ELF between Cs atoms and the other two kinds of atoms is almost equal to 0 (the Cs atoms are completely delocalized), while there is a polar covalent bond between Sn and Br atoms (ELF ≈ 0.5). The total charge density (Figure S1) shows covalent bonding behavior between Sn and Br.

The density functional perturbation method was used to calculate the second-order force constant matrix of the material along with the high symmetry point and phonon dispersion relationship of Cs_2SnBr_6. The primitive unit cell of Cs_2SnBr_6 is composed of nine atoms; 27 branches are generated at each phonon wave vector q, as shown in Figure 2(a). There is no virtual frequency mode in Cs_2SnBr_6, which proves that the material can exist stably, which is necessary to accurately obtain the second-order force constant required for the lattice thermal conductivity. The localization of these optical phonon branches is discernible from the atom-resolved phonon density of states (PDOS) (Figure 2(a)). A sharp localization of the phonon modes near 1 THz is observed, which is mainly due to the Cs atom, indicating the anharmonic rattling-like motion of Cs atoms in Cs_2SnBr_6. The localization of the phonon modes near 0.7 THz is also observed, where the Sn atom contributes significantly due to its heavier atomic mass, suggesting the dynamic rotation of the isolated $[SnBr_6]^{2-}$ octahedra. These two kinds of anharmonic vibrations trigger additional scattering between phonons, resulting in low lattice thermal conductivity.[4] Figure 2(b) shows the zoomed region of the low-frequency phonon dispersion of Cs_2SnBr_6. It is noted that several avoided crossings between the longitudinal acoustic

https://doi.org/10.1021/acs.jpclett.2c02350
J. Phys. Chem. Lett. 2022, 13, 9736−9744

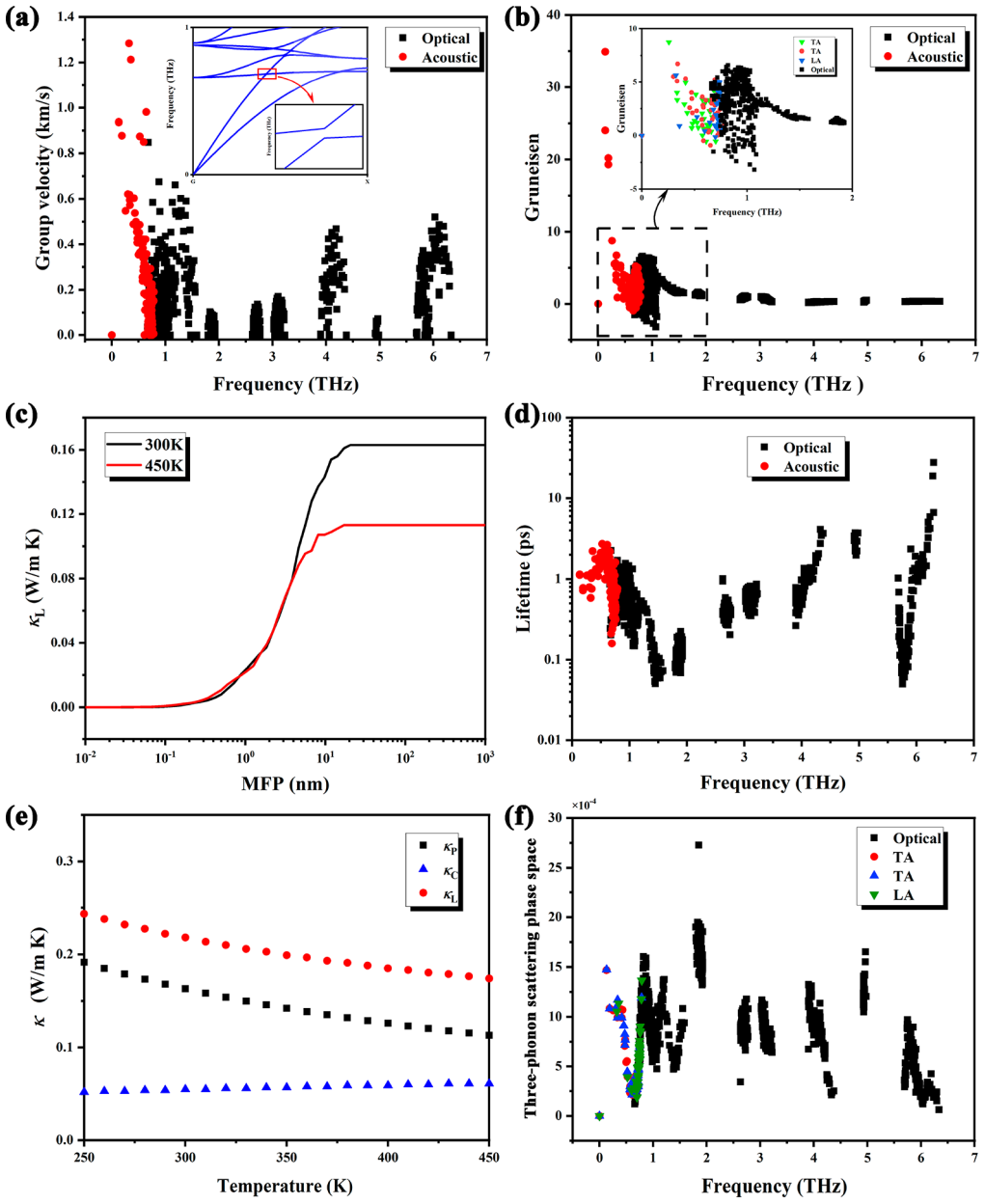

Figure 3. (a) Phonon group velocity, (b) Grüneisen parameter, (c) relationship between the cumulative lattice thermal conductivity and MFP, (d) anharmonic lifetime, (e) temperature-dependent thermal conductivities of Cs_2SnBr_6, (f) three-phonon scattering phase space as a function of frequency in the first Brillouin region.

(LA) phonon mode and the low-lying optical phonon mode within the range of 0.5−0.7 THz are present (highlighted by black circles). This phenomenon is due to the existence of rattling modes in the material, leading to strong anharmonic vibrations. A gap is overcome at the avoided crossing point in a two-level system with couplings. The avoided crossing is a manifestation of the coupling between two kinds of phonon mode branches,[10] in which the coupling strength is characterized by the gap at the avoided crossing point. In the vicinity of the avoided crossing point, there is strong hybridization between the optical and acoustic vibrations.

The temperature range for calculating the relevant properties is 300−450 K to ensure the stable existence of Cs_2SnBr_6 crystals.[11] We calculated the properties of phonon heat transport. The tendency of a rapid decrease of the phonon group velocity in the range of 0−1.5 THz, as shown in Figure 3(a), is due to the LO phonon mode couple with the LA phonon mode.[12] This avoidance of crossover between phonon modes leads to flattening of the acoustic phonons, and the average group velocity decreases (less than 2 km/s), which in turn causes a reduction of κ_L. The lowest group velocity is between 1.8 and 3.2 THz and 5 THz, corresponding to the almost straight-line flat dispersion curve in Figure 2(a). To quantify the anharmonicity, we calculated the Grüneisen parameters (Figure 3(b)) γ, describing the change of phonon eigenvalue according to the volume of the crystal cell, which is a direct measurement of the anharmonicity of the lattice vibration. In general, the larger the parameter, the stronger the anharmonicity of the material. The Grüneisen parameters of the strongly anharmonic solids are usually greater than 1.0,[13] such as PbTe (1.40).[14] The average value of γ reaches 1.86, and a considerably larger value of γ (>10) in the 0−0.5 THz

https://doi.org/10.1021/acs.jpclett.2c02350
J. Phys. Chem. Lett. 2022, 13, 9736−9744

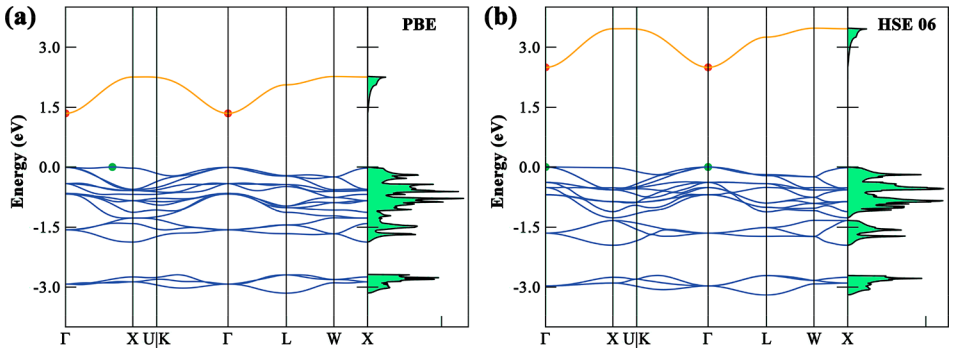

Figure 4. Calculated electronic band structures of Cs_2SnBr_6. The methods are (a) PBE and (b) HSE06, respectively.

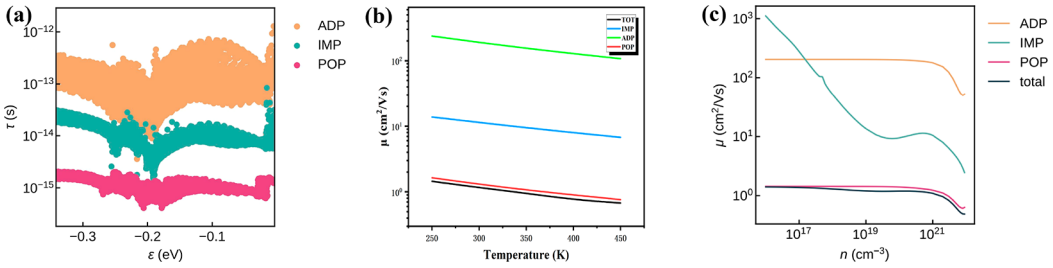

Figure 5. (a) Relaxation time and mobility of the hole associated with (b) the temperature and (c) the doping concentration, which is dominated by polar optical phonon scattering and ionized impurity scattering.

region is observed, indicating significant anharmonicity in the lattice. High anharmonicity in the system leads to slow propagation velocities and large phonon immersion, thus hindering phonon transport properties. Figure 3(c) shows the lattice thermal conductivity accumulating with the MFP, which reaches a plateau of 20.6 nm (17 nm) at 300 K (450 K). At room temperature, phonons with MFP < 9 nm make the majority contribution to the lattice thermal conductivity (~87.5%), of which the dominant contribution (~62%) comes from the phonons having MFP < 5 nm. The contribution of phonons in these MFP < 5 nm drastically increases to ~72% at 450 K, indicating that most of the lattice thermal conductivity is contributed by phonons with a mean free path less than 5 nm. This shows that the characteristic length of the nanostructure of the material is about 5 nm, which can further reduce the lattice thermal conductivity of the material. Figure 3(d) shows the phonon lifetime. The calculated phonon lifetime is in the range of 0.16−2.7 ps in Cs_2SnBr_6. Such a short phonon lifetime is rationalized by the processes of multiple phonon scattering. Because the dense low-order optical phonon mode permits many scattering paths (Figure 2(a)), the scattering from the low-energy optical phonons reduces their lifetime. In the glass-like crystal of Cs_2SnBr_6, the contribution of phonons to the lattice thermal conductivity consists of two parts. The first part is to obtain the lattice thermal conductivity of the particle-like conduction mechanism by iteratively solving the Boltzmann transport equation.[15,16] The second part is to use the Wigner transport equation to calculate the lattice thermal conductivity of the wave-like conduction mechanism.[17−19] The calculated thermal conductivity values as a function of temperature are plotted in Figure 3(e). At 300 K (450 K), the thermal conductivity of the particle-like κ_P accounts for 76% (64%) of the total thermal conductivity, and the thermal conductivity of the wave-like κ_C accounts for 24% (36%), respectively. This is because the highly anharmonic flat branches of compounds with guest atoms outside the center contribute to the coherence term. In this case, the influence of off-diagonal components of the heat-flux operator cannot be ignored, and the shortage of the Peierls−Boltzmanm heat transport equation for ultralow or glass-like thermal conductivity crystals can also be overcome. The lattice thermal conductivity ($\kappa_L = \kappa_P + \kappa_C$) from 0.21 W m^{-1} K^{-1} at room temperature decreases to 0.17 W m^{-1} K^{-1} near 450 K, which is obviously lower than other ultralow thermal conductivity materials with excellent thermoelectric properties, such as $AgInSe_2$ (300 K ~ 0.86 W m^{-1} K^{-1}),[20] Cs_2SnI_6 (300 K ~ 0.29 W m^{-1} K^{-1}),[3] SnSe (973 K ~ 0.23 W m^{-1} K^{-1}),[21] $CsAg_5Te_3$ (300 K ~ 0.27 W m^{-1} K^{-1}),[22] etc. The weighted phase space as a function of frequency for the system is shown in Figure 3(f), whose value is the number of three-phonon scattering. It is associated with the flattened phonon mode providing more phonon-scattering channels. They further demonstrate that the number of three-phonon scattering is relatively large over the entire frequency range, thereby preventing phonon thermal transport and reducing the lattice thermal conductivity. The large value of γ with high lattice anharmonicity also indicates enhanced phonon scattering and thereby reduces the lattice thermal conductivity κ_L.

In short, the strong anharmonicity of Cs_2SnBr_6 is proved by the fact that the Grüneisen parameter is greater than 1, the relaxation time is short, the group velocity is low, and the number of three-phonon scattering is large. The ultralow κ_L of Cs_2SnBr_6 originates from the strong anharmonicity caused by the rattling mode induced additional scattering between phonons, including Cs atomic vibrations and $[SnBr_6]^{2-}$ octahedral vibrations in the vacancy structure.

Figure 4 shows the band structures computed using the PBE and HSE06 functionals at equilibrium structures. They exhibit analogous band structures, the band gaps are 1.56 and 2.37 eV, and the latter approaches the experimental value (2.7 eV).[23] Below the valence band maximum (VBM), there are three

https://doi.org/10.1021/acs.jpclett.2c02350
J. Phys. Chem. Lett. 2022, 13, 9736−9744

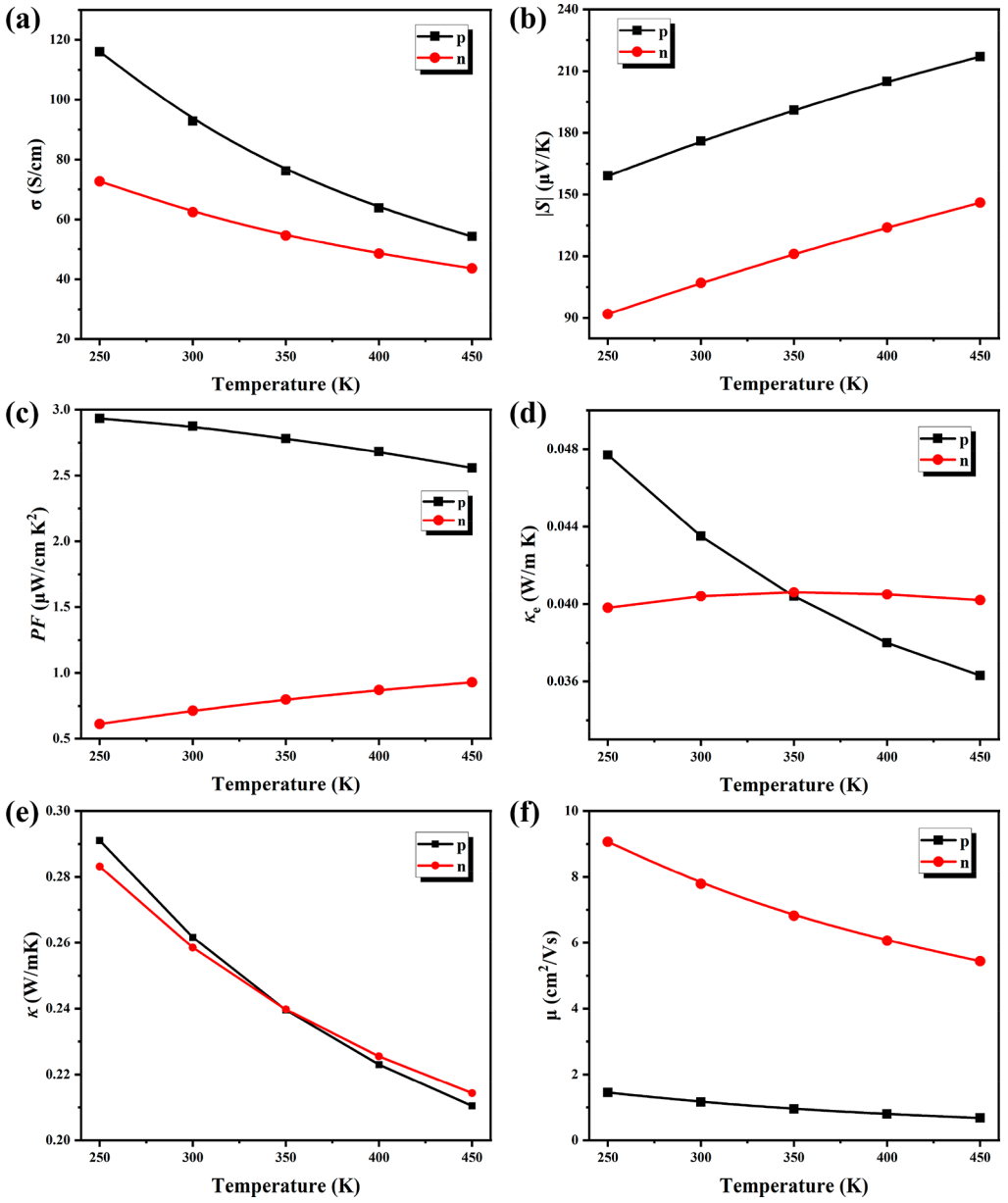

Figure 6. Thermoelectric properties of Cs_2SnBr_6. Temperature variation of the (a) conductivity, (b) absolute value of the Seebeck coefficient, (c) power factor (PF), (d) electron thermal conductivity (κ_e), (e) total thermal conductivity (κ), and (f) carrier mobility (μ) doped with electrons and holes for Cs_2SnBr_6. The electron doping concentration is 5×10^{19} cm^{-3}, and the hole doping concentration is 5×10^{20} cm^{-3}.

degenerate band valleys along the Γ−X, Γ−K, and Γ−L directions. The multienergy valley enhances the thermoelectric performance and is verified in many materials,[24] but the key to achieving high thermoelectric merit is the degree of energy band degeneracy.[25] Indeed, it can be seen that multiple degenerates exist on the valence band, so it is speculated that Cs_2SnBr_6 may be a *p*-type high-performance thermoelectric material.

Several recent studies have demonstrated that the carrier lifetime is also greatly affected by POP and IMP scattering.[26−28] Therefore, we calculate the electron transport properties considering the effects of three scattering mechanisms on the charge carriers. The parameters required for the relevant mechanisms can be found in the Supporting Information (Tables S1 and S2). Figure 5(a) shows the calculated relaxation time as a function of the electronic state energy at n = 5×10^{20} cm^{-3} and 450 K, doped electrons (n = 5×10^{19} cm^{-3}) (Figure S2), and the electronic state energy below the Fermi energy up to 0.6 eV (the zero-point energy set to $\varepsilon = \varepsilon_F$). From the contributions of various scattering mechanisms at the states close to the Fermi energy, it can be seen that POP scattering limits the carrier lifetime to remain around 1 fs compared to IMP (10 fs) and ADP (100 fs), demonstrating that electrons are greatly scattered by the optical phonons. Moreover, the comparison of doped holes and electrons at 300−400 K is calculated (Figures S3 and S4). Therefore, the previously estimated carrier lifetime[29] that is only scattered by acoustic deformations is not accurate enough.[30,31] Similarly, we also investigated the relaxation times with different doping concentrations at 450 K, as shown in Figures S5. It should be noted that the relaxation time under the ionized impurity scattering mechanism shows an overall shortening trend with the increase of the doping concentration, and the relaxation times under POP and ADP are almost

https://doi.org/10.1021/acs.jpclett.2c02350
J. Phys. Chem. Lett. 2022, 13, 9736−9744

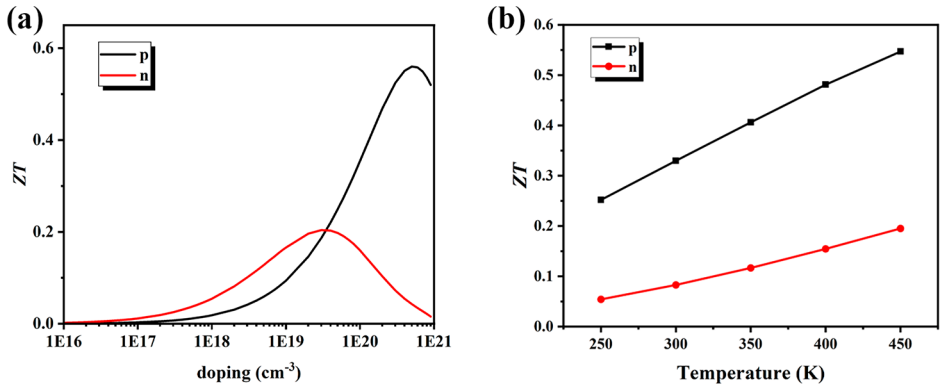

Figure 7. (a) Figure of merit (ZT) as a function of carrier concentration at 450 K. (b) ZT value as a function of temperature for comparative doping holes (electrons).

unchanged. Figure 5(b) shows the contributions of the three scattering mechanisms to the temperature-dependent mobility, where the mobility of doped electrons is larger than that of holes doped over the temperature range (Figure S6). It can be seen that the polar optical phonon scattering has a major contribution to the total mobility, resulting in the total mobility of 1 cm^2 V^{-1} s^{-1} for holes. The extremely low mobility is not favorable for the electron transport properties. Figure 5(c) shows the mobility as a function of the doping concentration for the three scattering mechanisms. The mobility under IMP scattering decreases rapidly with increasing the concentration at 300 K. We compared the mobility of the doped electrons and holes with the change of carrier concentration at 300−400 K, as shown in Figures S7 and S8. These results suggest that the mobility decreases with an increase in the temperature, which can also indirectly indicate that, for Cs_2SnBr_6, the increase in the temperature is not conducive to carrier transport.

Figure 6 shows the calculated Seebeck coefficient (S), electrical conductivity (σ), power factor (PF), electron thermal conductivity (κ_e), total thermal conductivity (κ), and mobility (μ) as a function of temperature for p- and n-type Cs_2SnBr_6. Cs_2SnBr_6 exhibits a metal-type behavior in the case of doping carriers, in which σ decreases with increasing the temperature. Compared to the classical high-performance thermoelectric materials, the electrical conductivity of Cs_2SnBr_6 is relatively low (SnSe-1500 S cm^{-1}).[32] The n-type (p-type) electrical conductivity of Cs_2SnBr_6 is about 62.4−43.6 S cm^{-1} (92.8−54.3 S cm^{-1}) at 300−450 K (Figure 6(a)). As shown in Figure 6(b), the p-type Seebeck coefficient is quite high, with a room-temperature value of 176 μV K^{-1}, which probably originates from the presence of the tin vacancies. On the other hand, for highly doped semiconductors, the magnitude of the Seebeck coefficient is usually determined by the density of states distribution around the Fermi level.[33] From Figure 2(b), the sharp valence band density of states and the convergence phenomenon in the valence band of Cs_2SnBr_6 lead to a larger p-type S compared to the n-type S.[34] The multiple degenerate valence band also proves that the Seebeck coefficient of p-type doping is higher than that of n-type doping. Figure 6(c) shows the peak power factor, indicating that the power factor in p-type is larger than that in n-type over a broad temperature range. The variation in the electronic thermal conductivity in Figure 6(d) shows the temperature dependence of κ_e for p-type Cs_2SnBr_6. The κ_e decreases from 0.04 W m^{-1} K^{-1} to 0.03 W m^{-1} K^{-1} in the 300−450 K temperature range. The room-temperature total thermal conductivity is 0.26 W m^{-1} K^{-1} (Figure 6(e)). Note that the κ_L is 0.21 W m^{-1} K^{-1} at 300 K, indicating that the key to quantifying the total thermal conductivity is still the lattice thermal conductivity. Figure 6(f) shows the mobility of the hole (electron). According to the calculation results, Cs_2SnBr_6 has a hole effective mass of 16 times that of an electron at point X (m_e = 0.451m_0, m_h = 7.961m_0), 8 times at point K and 7 times at point L (Table S3 in the Supporting Information). The effective mass of holes is much greater than that of electrons, resulting in a much higher mobility of electrons than holes. However, the high doping concentration of impurities (n = 5 × 10^{20} cm^{-3}) can balance the negative effect of low hole mobility on conductivity caused by the increase of effective mass. The calculated electron transport coefficient at 450 K as a function of doping concentration is shown in Figure S9. The electrical conductivity and the electron thermal conductivity have the same trend. They increase with the increase of the carrier concentration. The Seebeck coefficient decreases with the increase of the doping concentration. Due to the structure defects, the mobility of both doped electrons and holes is relatively small; in particular, the hole transport is greatly inhibited, resulting in the power factor of the doped p-type being only twice that of the heavily doped electron case. As PBE severely underestimates the band gap, the electronic structures calculated by HSE06 are used to calculate the electronic transport properties. The differences in electron transport correlation coefficients calculated for PBE and HSE06 are shown in Figure S10. The formula for calculating the relevant electron transport properties is detailed in the Supporting Information.

The dimensionless thermoelectric figure of merit is further evaluated based on the calculated transport coefficients and lattice thermal conductivity of Cs_2SnBr_6. It can be seen that ZT peaks at a certain range of the doping concentrations from Figure 7(a), which is consistent with the optimal carrier concentration. The peak value of p-type ZT is calculated to be 0.55, and that of n-type ZT is 0.20. Figure 7(b) displays the temperature dependence of ZT under doping of two kinds of carriers. The ZT increases monotonically with increasing temperature, which is consistent with the dependence of the Seebeck coefficient on temperature. The large Seebeck coefficient of the p-doped carriers in the materials leads to a larger ZT compared to that of the n-type doped carriers. This reveals that Cs_2SnBr_6 becomes an p-type semiconductor with a

https://doi.org/10.1021/acs.jpclett.2c02350
J. Phys. Chem. Lett. 2022, 13, 9736−9744

high level of hole doping. This verifies the previous assumption that Cs_2SnBr_6 is a good thermoelectric material.

In summary, we achieved a complete ab initio prediction of the thermoelectric figure of merit for Cs_2SnBr_6 by calculating the electrical and thermal transport properties based on first-principles methods. We use the Wigner transport equation to solve the lattice thermal conductor from the off-diagonal contribution caused by the wavy conduction mechanism for complex crystals. It is found that the strong anharmonicity leads to the material exhibiting ultralow lattice thermal conductivity (0.17 W m^{-1} K^{-1} ~ 450 K). In addition, the electrical transport properties show that the high Seebeck coefficient value of the doped *p*-type carriers reaches 217 μV K^{-1}. The ultralow lattice thermal conductivity and a high Seebeck coefficient help to reach the ZT value of 0.55 at 450 K. The study unveiled that Cs_2SnBr_6, with ultralow lattice thermal conductivity, is a promising *p*-type thermoelectric material, and it also helps us understand the ultralow κ_L in complex crystals with strong anharmonicity and find new thermoelectricity materials.

COMPUTATIONAL DETAILS

The first-principles calculations were implemented in the Vienna ab initio simulation package (VASP).[35,36] The exchange-correlation energy adopting PBE[36] in the generalized gradient approximation form was employed to deal with the exchange-correlation functional. The Heyd−Suseria−Ernzerhof HSE06[37] method was employed to obtain an accurate band gap and electronic transport performance, and the projection enhanced wave (PAW)[38] pseudopotential was used as the basis for representing the wave function. The kinetic energy cutoff is 500 eV,[39,40] and the Brillouin zone integral is calculated using a 5 × 5 × 5 k-point grid[41] for self-consistent and non-self-consistent calculations. The geometry structure was fully relaxed, with a criterion of convergence for residual forces of 0.001 eV/Å, and the total energy difference converged to within 10^{-4} eV. The electronic transport properties of Cs_2SnBr_6 were calculated by solving the Boltzmann transport equation, utilizing the AMSET[42] package. We use the Wigner transport equation[17,19] to calculate the thermal conductivity of the material, including the particle-like propagation mechanism of phonon wavepackets discussed by Peierls for crystals and the wave-like interband conduction mechanism discussed by Allen and Feldman for harmonic glasses. The particle-like thermal conductivity is calculated using the ShengBTE[43] code, using the Phonopy[15] and Thirdorder codes to calculate the correlation force constant matrix as input to ShengBTE. We convert the force constants from ShengBTE format to Phono3py[44] format using hiPhive,[45] and the wave-like thermal conductivity is computed using the software Phono3py to solve the Wigner transport equation. The density functional perturbation theory method[46] was chosen to calculate the phonon dispersion relations and second-order force constants for Cs_2SnBr_6. The harmonic and third-order force constant matrices are calculated using the real-space supercell method in 2 × 2 × 2 supercells (72 atoms) with a 3 × 3 × 3 k-points mesh. After testing, the interactions including the sixth nearest neighbor atoms were considered to strictly meet the convergence criteria.

ASSOCIATED CONTENT

Supporting Information

The Supporting Information is available free of charge at https://pubs.acs.org/doi/10.1021/acs.jpclett.2c02350.

Computational details under other conditions, including: total charge density, relaxation time, mobility, and electron transport coefficient (PDF)

AUTHOR INFORMATION

Corresponding Authors

Laizhi Sui − *State Key Laboratory of Molecular Reaction Dynamics and Dalian Coherent Light Source, Dalian Institute of Chemical Physics, Chinese Academy of Sciences, Dalian 116023, China;* orcid.org/0000-0003-3459-9755; Email: lzsui@dicp.ac.cn

Anmin Chen − *Institute of Atomic and Molecular Physics, Jilin University, Changchun 130012, China*; Email: amchen@jlu.edu.cn

Kaijun Yuan − *State Key Laboratory of Molecular Reaction Dynamics and Dalian Coherent Light Source, Dalian Institute of Chemical Physics, Chinese Academy of Sciences, Dalian 116023, China;* orcid.org/0000-0002-5108-8984; Email: kjyuan@dicp.ac.cn

Authors

Xiangyu Zeng − *Institute of Atomic and Molecular Physics, Jilin University, Changchun 130012, China; State Key Laboratory of Molecular Reaction Dynamics and Dalian Coherent Light Source, Dalian Institute of Chemical Physics, Chinese Academy of Sciences, Dalian 116023, China*

Jutao Jiang − *State Key Laboratory of Molecular Reaction Dynamics and Dalian Coherent Light Source, Dalian Institute of Chemical Physics, Chinese Academy of Sciences, Dalian 116023, China*

Guangming Niu − *State Key Laboratory of Molecular Reaction Dynamics and Dalian Coherent Light Source, Dalian Institute of Chemical Physics, Chinese Academy of Sciences, Dalian 116023, China; Marine Engineering College, Dalian Maritime University, Dalian 116026, China*

Yutong Zhang − *State Key Laboratory of Molecular Reaction Dynamics and Dalian Coherent Light Source, Dalian Institute of Chemical Physics, Chinese Academy of Sciences, Dalian 116023, China*

Xiaowei Wang − *State Key Laboratory of Molecular Reaction Dynamics and Dalian Coherent Light Source, Dalian Institute of Chemical Physics, Chinese Academy of Sciences, Dalian 116023, China*

Xin Liu − *State Key Laboratory of Molecular Reaction Dynamics and Dalian Coherent Light Source, Dalian Institute of Chemical Physics, Chinese Academy of Sciences, Dalian 116023, China; Department of Physics, School of Science, Dalian Maritime University, Dalian 116026, China*

Mingxing Jin − *Institute of Atomic and Molecular Physics, Jilin University, Changchun 130012, China*

Complete contact information is available at: https://pubs.acs.org/10.1021/acs.jpclett.2c02350

Notes

The authors declare no competing financial interest.

https://doi.org/10.1021/acs.jpclett.2c02350
J. Phys. Chem. Lett. 2022, 13, 9736−9744

■ ACKNOWLEDGMENTS

This work was supported by the Chemical Dynamics Research Center (Grant No. 22288201), the National Natural Science Foundation of China (NSFC Nos. 21873009, 21922306), the Key Technology Team of the Chinese Academy of Science (Grant No. GJJSTD20220001), and the Liaoning Revitalization Talents Program (XLYC1907154).

■ REFERENCES

(1) Gorai, P.; Stevanović, V.; Toberer, E. S. Computationally guided discovery of thermoelectric materials. *Nat. Rev. Mater.* **2017**, *2* (9), 17053.
(2) Lee, W.; Li, H.; Wong, A. B.; Zhang, D.; Lai, M.; Yu, Y.; Kong, Q.; Lin, E.; Urban, J. J.; Grossman, J. C.; Yang, P. Ultralow thermal conductivity in all-inorganic halide perovskites. *Proc. Natl. Acad. Sci. U. S. A.* **2017**, *114* (33), 8693−8697.
(3) Bhui, A.; Ghosh, T.; Pal, K.; Singh Rana, K.; Kundu, K.; Soni, A.; Biswas, K. Intrinsically Low Thermal Conductivity in the n-Type Vacancy-Ordered Double Perovskite Cs_2SnI_6: Octahedral Rotation and Anharmonic Rattling. *Chem. Mater.* **2022**, *34* (7), 3301−3310.
(4) Li, J.; Hu, W.; Yang, J. High-Throughput Screening of Rattling-Induced Ultralow Lattice Thermal Conductivity in Semiconductors. *J. Am. Chem. Soc.* **2022**, *144* (10), 4448−4456.
(5) Sajjad, M.; Mahmood, Q.; Singh, N.; Larsson, J. A. Ultralow Lattice Thermal Conductivity in Double Perovskite Cs_2PtI_6: A Promising Thermoelectric Material. *ACS Appl. Energy Mater.* **2020**, *3* (11), 11293−11299.
(6) Fallah, M.; Milani Moghaddam, H. Ultra-low lattice thermal conductivity and high thermoelectric efficiency in Cs_2SnX_6 (X = Br, I): A DFT study. *Mater. Sci. Semicond. Process.* **2021**, *133*, 105984.
(7) Chen, W.; Pöhls, J.-H.; Hautier, G.; Broberg, D.; Bajaj, S.; Aydemir, U.; Gibbs, Z. M.; Zhu, H.; Asta, M.; Snyder, G. J.; Meredig, B.; White, M. A.; Persson, K.; Jain, A. Understanding thermoelectric properties from high-throughput calculations: trends, insights, and comparisons with experiment. *J. Mater. Chem. C* **2016**, *4* (20), 4414−4426.
(8) Huang, S.; Wang, Z.; Xiong, R.; Yu, H.; Shi, J. Significant enhancement in thermoelectric performance of Mg_3Sb_2 from bulk to two-dimensional mono layer. *Nano Energy* **2019**, *62*, 212−219.
(9) Xie, Q.-Y.; Liu, P.-F.; Ma, J.-J.; Kuang, F.-G.; Zhang, K.-W.; Wang, B.-T. Monolayer SnI_2: An Excellent p-Type Thermoelectric Material with Ultralow Lattice Thermal Conductivity. *Materials* **2022**, *15* (9), 3147.
(10) Li, W.; Carrete, J.; Madsen, G. K. H.; Mingo, N. Influence of the optical-acoustic phonon hybridization on phonon scattering and thermal conductivity. *Phys. Rev. B* **2016**, *93* (20), 205203.
(11) Belessiotis, G. V.; Arfanis, M.; Kaltzoglou, A.; Likodimos, V.; Raptis, Y. S.; Falaras, P.; Kontos, A. G. Temperature effects on the vibrational properties of the Cs_2SnX_6 'defect' perovskites (X = I, Br, Cl). *Mater. Chem. Phys.* **2021**, *267*, 124679.
(12) Zhao, L.-D.; Lo, S.-H.; Zhang, Y.; Sun, H.; Tan, G.; Uher, C.; Wolverton, C.; Dravid, V. P.; Kanatzidis, M. G. Ultralow thermal conductivity and high thermoelectric figure of merit in SnSe crystals. *Nature.* **2014**, *508* (7496), 373−377.
(13) Toberer, E. S.; Zevalkink, A.; Snyder, G. J. Phonon engineering through crystal chemistry. *J. Mater. Chem.* **2011**, *21* (40), 15843.
(14) Morelli, D. T.; Jovovic, V.; Heremans, J. P. Intrinsically Minimal Thermal Conductivity in Cubic I-V-VI_2 Semiconductors. *Phys. Rev. Lett.* **2008**, *101* (3), 035901.
(15) Togo, A.; Tanaka, I. First principles phonon calculations in materials science. *Scr. Mater.* **2015**, *108*, 1−5.
(16) McGaughey, A. J. H.; Jain, A.; Kim, H.-Y. Phonon properties and thermal conductivity from first principles, lattice dynamics, and the Boltzmann transport equation. *J. Appl. Phys.* **2019**, *125* (1), 011101.
(17) Simoncelli, M.; Marzari, N.; Mauri, F. Unified theory of thermal transport in crystals and glasses. *Nat. Phys.* **2019**, *15* (8), 809−813.
(18) Caldarelli, G.; Simoncelli, M.; Marzari, N.; Mauri, F.; Benfatto, L. Many-body Green's function approach to lattice thermal transport. *Phys. Rev. B* **2022**, *106* (2), 024312.
(19) Simoncelli, M.; Marzari, N.; Mauri, F. Wigner formulation of thermal transport in solids. *Phys. Rev. X* **2022**.
(20) Zhu, Y.; Wei, B.; Liu, J.; Koocher, N. Z.; Li, Y.; Hu, L.; He, W.; Deng, G.; Xu, W.; Wang, X.; Rondinelli, J. M.; Zhao, L.-D.; Snyder, G. J.; Hong, J. Physical insights on the low lattice thermal conductivity of $AgInSe_2$. *Mater. Today Phys.* **2021**, *19*, 100428.
(21) Zhao, L.-D.; Lo, S.-H.; Zhang, Y.; Sun, H.; Tan, G.; Uher, C.; Wolverton, C.; Dravid, V. P.; Kanatzidis, M. G. Ultralow thermal conductivity and high thermoelectric figure of merit in SnSe crystals. *Nature.* **2014**, *508* (7496), 373−377.
(22) Jong, U. G.; Kang, C. J.; Kim, S. Y.; Kim, H. C.; Yu, C. J. Superior thermoelectric properties of ternary chalcogenides $CsAg_5Q_3$ (Q = Te, Se) predicted using first-principles calculations. *Phys. Chem. Chem. Phys.* **2022**, *24* (9), 5729−5737.
(23) Kaltzoglou, A.; Antoniadou, M.; Kontos, A. G.; Stoumpos, C. C.; Perganti, D.; Siranidi, E.; Raptis, V.; Trohidou, K.; Psycharis, V.; Kanatzidis, M. G.; Falaras, P. Optical-Vibrational Properties of the Cs_2SnX_6 (X = Cl, Br, I) Defect Perovskites and Hole-Transport Efficiency in Dye-Sensitized Solar Cells. *J. Phys. Chem. C* **2016**, *120* (22), 11777−11785.
(24) Wang, D.; He, W.; Chang, C.; Wang, G.; Wang, J.; Zhao, L.-D. Thermoelectric transport properties of rock-salt SnSe: first-principles investigation. *J. Mater. Chem. C* **2018**, *6* (44), 12016−12022.
(25) Zhao, L.-D.; Dravid, V. P.; Kanatzidis, M. G. The panoscopic approach to high performance thermoelectrics. *Energy Environ. Sci.* **2014**, *7* (1), 251−268.
(26) Ma, J.; Chen, Y.; Li, W. Intrinsic phonon-limited charge carrier mobilities in thermoelectric SnSe. *Phys. Rev. B* **2018**, *97* (20), 205207.
(27) Cao, J.; Querales-Flores, J. D.; Murphy, A. R.; Fahy, S.; Savić, I. Dominant electron-phonon scattering mechanisms in n-type PbTe from first principles. *Phys. Rev. B* **2018**, *98* (20), 205202.
(28) Pohls, J. H.; Chanakian, S.; Park, J.; Ganose, A. M.; Dunn, A.; Friesen, N.; Bhattacharya, A.; Hogan, B.; Bux, S.; Jain, A.; Mar, A.; Zevalkink, A. Experimental validation of high thermoelectric performance in $RECuZnP_2$ predicted by high-throughput DFT calculations. *Mater. Horiz.* **2021**, *8* (1), 209−215.
(29) Bardeen, J.; Shockley, W. Deformation Potentials and Mobilities in Non-Polar Crystals. *Phys. Rev.* **1950**, *80* (1), 72−80.
(30) Jiang, J.; Pan, Y.; Zhou, T.; Niu, Y.; Kong, X.; Song, J.; Yang, C.; Yu, Y.; Wang, C. The comprehensive first-principle study of the thermoelectric performance of p- and n-type SnS. *Mater. Today Commun.* **2020**, *24*, 101167.
(31) Guo, R.; Wang, X.; Kuang, Y.; Huang, B. First-principles study of anisotropic thermoelectric transport properties of IV-VI semiconductor compounds SnSe and SnS. *Phys. Rev. B* **2015**, *92* (11), 115202.
(32) Tan, G.; Zhao, L. D.; Kanatzidis, M. G. Rationally Designing High-Performance Bulk Thermoelectric Materials. *Chem. Rev.* **2016**, *116* (19), 12123−12149.
(33) Wang, D.; Tang, L.; Long, M.; Shuai, Z. First-principles investigation of organic semiconductors for thermoelectric applications. *J. Chem. Phys.* **2009**, *131* (22), 224704.
(34) Hao, S.; Shi, F.; Dravid, V. P.; Kanatzidis, M. G.; Wolverton, C. Computational Prediction of High Thermoelectric Performance in Hole Doped Layered GeSe. *Chem. Mater.* **2016**, *28* (9), 3218−3226.
(35) Kresse, G.; Furthmüller, J. Efficient iterative schemes for ab initio total-energy calculations using a plane-wave basis set. *Phys. Rev. B* **1996**, *54* (16), 11169−11186.
(36) Perdew, J. P.; Ruzsinszky, A.; Csonka, G. I.; Vydrov, O. A.; Scuseria, G. E.; Constantin, L. A.; Zhou, X.; Burke, K. Restoring the density-gradient expansion for exchange in solids and surfaces. *Phys. Rev. Lett.* **2008**, *100* (13), 136406.
(37) Heyd, J.; Scuseria, G. E. Assessment and validation of a screened Coulomb hybrid density functional. *J. Chem. Phys.* **2004**, *120* (16), 7274−80.

https://doi.org/10.1021/acs.jpclett.2c02350
J. Phys. Chem. Lett. 2022, 13, 9736−9744

(38) Blochl, P. E. Projector augmented-wave method. *Phys. Rev., B Condens. Matter* **1994**, *50* (24), 17953−17979.
(39) Kleinman, L.; Bylander, D. M. Efficacious Form for Model Pseudopotentials. *Phys. Rev. Lett.* **1982**, *48* (20), 1425−1428.
(40) Troullier, N.; Martins, J. L. Efficient pseudopotentials for plane-wave calculations. *Phys. Rev. B* **1991**, *43* (3), 1993−2006.
(41) Monkhorst, H. J.; Pack, J. D. Special points for Brillouin-zone integrations. *Phys. Rev. B* **1976**, *13* (12), 5188−5192.
(42) Ganose, A. M.; Park, J.; Faghaninia, A.; Woods-Robinson, R.; Persson, K. A.; Jain, A. Efficient calculation of carrier scattering rates from first principles. *Nat. Commun.* **2021**, *12* (1), 2222.
(43) Li, W.; Carrete, J.; Katcho, N. A.; Mingo, N. ShengBTE: A solver of the Boltzmann transport equation for phonons. *Comput. Phys. Commun.* **2014**, *185* (6), 1747−1758.
(44) Togo, A.; Chaput, L.; Tanaka, I. Distributions of phonon lifetimes in Brillouin zones. *Phys. Rev. B* **2015**, *91* (9), 094306.
(45) Eriksson, F.; Fransson, E.; Erhart, P. The Hiphive Package for the Extraction of High-Order Force Constants by Machine Learning. *Adv. Theory Simul.* **2019**, *2* (5), 1800184.
(46) Baroni, S.; de Gironcoli, S.; Dal Corso, A.; Giannozzi, P. Phonons and related crystal properties from density-functional perturbation theory. *Rev. Mod. Phys.* **2001**, *73* (2), 515−562.

https://doi.org/10.1021/acs.jpclett.2c02350
J. Phys. Chem. Lett. 2022, 13, 9736−9744